ARTICLES
https://doi.org/10.1038/s41567-021-01394-x
nature physics

Check for updates

OPEN

Precise determination of the B_s^0–$\overline{B}_s^0$ oscillation frequency

LHCb collaboration*

Mesons comprising a beauty quark and strange quark can oscillate between particle (B_s^0) and antiparticle ($\overline{B}_s^0$) flavour eigenstates, with a frequency given by the mass difference between heavy and light mass eigenstates, Δm_s. Here we present a measurement of Δm_s using $B_s^0 \to D_s^- \pi^+$ decays produced in proton–proton collisions collected with the LHCb detector at the Large Hadron Collider. The oscillation frequency is found to be $\Delta m_s = 17.7683 \pm 0.0051 \pm 0.0032\,\text{ps}^{-1}$, where the first uncertainty is statistical and the second is systematic. This measurement improves on the current Δm_s precision by a factor of two. We combine this result with previous LHCb measurements to determine $\Delta m_s = 17.7656 \pm 0.0057\,\text{ps}^{-1}$, which is the legacy measurement of the original LHCb detector.

Neutral mesons with strange, charm or beauty quantum numbers can mix with their antiparticles, as these quantum numbers are not conserved by the weak interaction. The neutral meson comprising an antibeauty quark and a strange quark, namely, the B_s^0 meson, and its antiparticle, namely, the $\overline{B}_s^0$ meson, are one such example. In the B_s^0–$\overline{B}_s^0$ system, the observed particle and antiparticle states are linear combinations of the heavy (H) and light (L) mass eigenstates. These mass eigenstates have corresponding masses m_H and m_L and decay widths Γ_H and Γ_L (ref. [1]). As a consequence, the B_s^0–$\overline{B}_s^0$ system oscillates with a frequency given by the mass difference, $\Delta m_s = m_H - m_L$. This oscillation frequency is an important parameter of the standard model of particle physics. In combination with the B^0–$\overline{B}^0$ oscillation frequency, Δm_d, it provides a powerful constraint on the Cabibbo–Kobayashi–Maskawa quark-mixing matrix[2–6]. A precise measurement of Δm_s is also required to reduce the systematic uncertainty associated with measurements of matter–antimatter differences in the B_s^0–$\overline{B}_s^0$ system[7].

In this Article, we present a measurement of Δm_s using B_s^0 mesons that decay to a charmed–strange D_s^- meson and a pion, $B_s^0 \to D_s^- \pi^+$, and decays with the opposite charge, $\overline{B}_s^0 \to D_s^- \pi^+$. We refer to both charge combinations as $B_s^0 \to D_s^- \pi^+$ throughout the paper, and similarly for decays of the D_s^- meson. The measurement is performed using data collected between 2015 and 2018, denoted as Run 2 of the Large Hadron Collider (LHC), corresponding to an integrated luminosity of 6 fb^{-1} of proton–proton (pp) collisions at a centre-of-mass energy of 13 TeV.

The first measurement in which the significance of the observed B_s^0–$\overline{B}_s^0$ oscillation signal exceed five standard deviations was obtained by the CDF collaboration[8]. More recently, the LHCb collaboration has performed several measurements of Δm_s using data collected at the LHC: a measurement using $B_s^0 \to D_s^- \pi^+$ decays[9]; two measurements using $B_s^0 \to J/\psi K^+ K^-$ decays[10,11]; and a measurement using $B_s^0 \to D_s^{\mp} \pi^{\pm} \pi^{\pm} \pi^{\mp}$ decays[12]. Theoretical predictions for Δm_s are available[6,13–17], with the most precise prediction provided in ref. [18]. The prediction is consistent with—but considerably less precise than—existing experimental results.

The $B_s^0 \to D_s^- \pi^+$ decay time distribution, in the absence of detector effects, can be written as

$$P(t) \approx e^{-\Gamma_s t}\left[\cosh\left(\frac{\Delta\Gamma_s t}{2}\right) + C\cos(\Delta m_s t)\right], \qquad (1)$$

where $\Gamma_s = (\Gamma_H + \Gamma_L)/2$ is the B_s^0 meson decay width and $\Delta\Gamma_s = \Gamma_H - \Gamma_L$ is the decay-width difference between the heavy and light mass eigenstates. The parameter C takes the value $C = 1$ for unmixed decays, that is, $B_s^0 \to D_s^- \pi^+$, and $C = -1$ for decays in which the initially produced meson mixed into its antiparticle before decaying, that is, $B_s^0 \to \overline{B}_s^0 \to D_s^- \pi^+$. The mixed decay is referred to as $\overline{B}_s^0 \to D_s^- \pi^+$ throughout the paper. The mass difference Δm_s corresponds to a frequency in natural units, and is measured in inverse picoseconds (ps^{-1}).

The LHCb detector[19,20] is designed to study the decays of beauty and charm hadrons produced in pp collisions at the LHC. It instruments a region around the proton beam axis, covering the polar angles between 10 and 250 mrad, in which approximately a quarter of the b-hadron decay products are fully contained. The detector includes a high-precision tracking system with a dipole magnet, providing measurements of the momentum and decay-vertex position of particles. Different types of charged particle are distinguished using information from two ring-imaging Cherenkov detectors, a calorimeter and a muon system.

Simulated samples of $B_s^0 \to D_s^- \pi^+$ decays and data control samples are used to verify the analysis procedure and to study systematic effects. The simulation provides a detailed model of the experimental conditions, including the pp collision, decays of the produced particles, their final-state radiation and response of the detector. Simulated samples are corrected for residual differences in relevant kinematic distributions to improve the agreement with data. The software used is described in refs. [21–27].

The B_s^0 mesons travel a macroscopic distance at LHC energies (1 cm on average) before decaying and are considerably heavier than most other particles produced directly in pp collisions. Thus, their decay products have large displacement relative to the pp collision point and a larger momentum transverse to the beam axis compared with other particles. The candidate selection exploits these fundamental properties. Two fast real-time selections use partial detector information to reject LHC bunch crossings likely to be incompatible with the presence of the signal, before a third selection uses fully aligned and calibrated data in real time to reconstruct

*A list of authors and their affiliations appears online only.

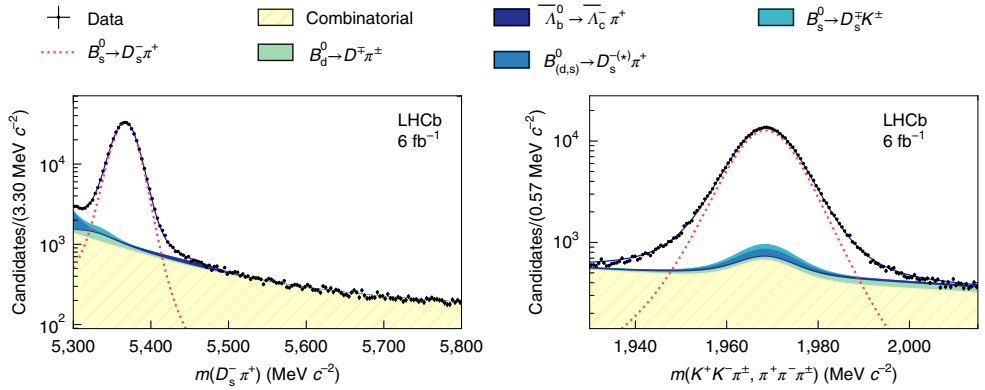

Fig. 1 | Invariant mass distributions. Distributions of the $D_s^- \pi^+$ (left) and $K^+K^-\pi^\pm$ or $\pi^+\pi^-\pi^\pm$ (right) invariant mass for the selected candidates, namely, $m(D_s^- \pi^+)$ and $m(K^+K^-\pi^\pm, \pi^+\pi^-\pi^\pm)$, respectively. The mass fit described in the text is overlaid. The different contributions are shown as coloured areas (for the background) or by dashed lines (for the signal). The vertical bars, typically visible only in regions with low numbers of candidates, correspond to the statistical uncertainty in the number of observed candidates in each bin. The horizontal bin width is indicated on the vertical axis legend.

and select topologies consistent with the signal[28]. Selected collisions are recorded to permanent storage. All selections, except the first real-time selection, are based on multivariate classifiers. Two subsequent selections fully reconstruct the decays with the D_s^- meson reconstructed in both $K^-K^+\pi^-$ and $\pi^-\pi^+\pi^-$ final states. After the real-time stages, the initial 'offline' selection is based on track kinematic quantities and displacement relative to the pp collision point that favours the signal, followed by a multivariate classifier trained on properties of the full signal decay. These selections sequentially improve the signal purity of the sample to the final value of 84%, which is optimized using a simulation to maximize the product of signal significance and signal efficiency. This criterion gives the optimal sensitivity to the oscillation frequency.

The remaining sources of background after selection consist of random track combinations (combinatorial background); $B_s^0 \to D_s^{*-} \pi^+$ decays, where the photon from the $B_s^0 \to D_s^- \gamma$ decay is not reconstructed; and contributions from b-hadron decays with similar topologies to the signal, namely, $B^0 \to D^- \pi^+$, $\overline{\Lambda}_b^0 \to \overline{\Lambda}_c^- \pi^+$ and $B_s^0 \to D_s^\mp K^\pm$ decays. Decays with similar topology are suppressed by applying kinematic vetoes and additional particle identification requirements.

To measure Δm_s, a $B_s^0 \to D_s^- \pi^+$ decay time distribution is first constructed in the absence of a background. This is achieved by performing an unbinned two-dimensional likelihood fit to the observed $D_s^- \pi^+$ and $K^-K^+\pi^-$ or $\pi^-\pi^+\pi^-$ invariant mass distributions. This fit is used to determine the signal yield and a set of weights[29] used to statistically subtract the background in the subsequent fit to the decay time distribution. The invariant mass distributions of the selected decays are shown in Fig. 1. The non-peaking contribution in the combinatorial background distribution, as shown in Fig. 1 (right), is due to events in which a fake D_s^- candidate is produced from a combination of random tracks. The peaking contribution is due to genuine D_s^- candidates combined with a random track resulting in a fake B_s^0 candidate.

The probability density functions describing the invariant mass distributions of the signal and background are obtained using a mixture of control samples in the data and simulation. The $D_s^- \pi^+$ and $K^-K^+\pi^-$ or $\pi^-\pi^+\pi^-$ invariant-mass signal shapes are described by the sum of Hypatia[30] and Johnson S_U (ref. [31]) functions. The combinatorial background contribution for both invariant mass distributions is described by an exponential function in each of them with the parameters determined in the fit. The $B^0 \to D^- \pi^+$, $\overline{\Lambda}_b^0 \to \overline{\Lambda}_c^- \pi^+$ or $B_s^0 \to D_s^\mp K^\pm$ background components constitute less than 2% of the signal yield and are accounted for in the fit to the invariant mass distributions using yields obtained from known branching fractions and relative efficiencies, as determined from the simulated samples, which are weighted to account for differences between the data and simulation. The $B^0 \to D_s^- \pi^+$ and $B_s^0 \to D_s^{*-} \pi^+$ background components are also obtained from the simulated samples and included in the mass fit. The combined $B^0 \to D_s^- \pi^+$ and $B_s^0 \to D_s^{*-} \pi^+$ yield is a free parameter of the fit. The signal yield obtained from the invariant mass fit is $378{,}700 \pm 700$.

Decay time parameterization (equation (1)) is modified to account for the following detector effects: decay-time-dependent reconstruction efficiency; time-dependent decay time resolution; imperfect knowledge of the initial flavour of the reconstructed B_s^0 or $\overline{B}_s^0$ meson; asymmetry in B_s^0 or $\overline{B}_s^0$ production in pp collisions; and asymmetry in the reconstruction of final-state particles due to interactions in the detector material[32].

Due to the lifetime biasing effect of the selections, the reconstruction efficiency is low at small decay times and increases to a plateau after 2 ps. The decay-time-dependent reconstruction efficiency is modelled with cubic b-spline curves as described

Table 1 | Systematic uncertainties affecting the measurement of Δm_s

Description	Systematic uncertainty (ps^{-1})
Reconstruction effects:	
Momentum-scale uncertainty	0.0007
Detector length scale	0.0018
Detector misalignment	0.0020
Invariant-mass fit model:	
Background parameterization	0.0002
$B_s^0 \to D_s^{*-} \pi^+$ and $B^0 \to D_s^- \pi^+$ contributions	0.0005
Decay-time fit model:	
Decay-time resolution model	0.0011
Neglecting correlation among observables	0.0011
Cross-checks:	
Kinematic correlations	0.0003
Total systematic uncertainty	0.0032

Sources of systematic uncertainties are discussed in the text. Additional details are provided in Methods. The total systematic uncertainty is obtained by adding the contributions in quadrature.

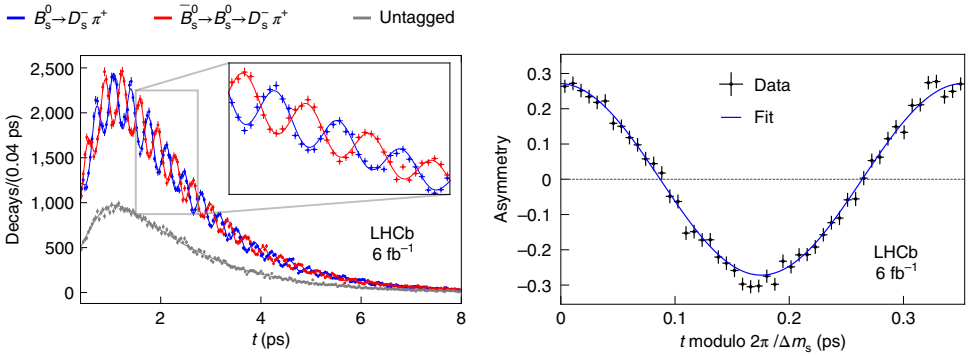

Fig. 2 | Decay time distribution of the signal decays. Distribution of the decay time of the $B_s^0 \to D_s^- \pi^+$ signal decays (left) and decay time asymmetry between the mixed and unmixed signal decays (right). The vertical bars correspond to the statistical uncertainty in the number of observed candidates in each bin. The horizontal bars represent the bin width. In the left plot, the horizontal bin width is indicated on the vertical axis legend. The three components—unmixed, mixed and untagged—are shown in blue, red and grey, respectively. The inset shows a zoomed-in view of the region delineated in grey. The fit described in the text is overlaid.

elsewhere[33]. The spline coefficients are allowed to vary in the fit to the observed decay time distribution.

The decay time resolution is measured using a data sample of D_s^- mesons originating from pp interactions without being required to come from an intermediate B_s^0 meson decay. These 'prompt' candidates pass the same real-time selection procedure as the signal sample. After real-time selection, additional requirements are applied to ensure the selection of a D_s^- signal peak with high background rejection but without any requirement on displacement from the pp collision point. The multivariate classifier trained using the full signal decay is not applied. The reconstructed decay time in this control sample is proportional to the distance between the D_s^- production vertex and an artificial B_s^0 decay vertex, formed by combining the prompt D_s^- meson with a π^+ track from the same pp collision. It is, therefore, compatible with a zero decay time up to bias and resolution effects. A linear relationship is observed between the decay time resolution measured at zero decay time and the decay time uncertainty estimated in the vertex fit. This relationship is used to calibrate the $B_s^0 \to D_s^- \pi^+$ decay time uncertainty. Simulated prompt D_s^- and $B_s^0 \to D_s^- \pi^+$ decays, for which the generated decay time is known, are used to check the suitability of this method, which determines a 0.005 ps bias in the reconstructed decay time due to residual detector misalignments. This bias is corrected in the analysis. The uncertainty in Δm_s due to these residual detector misalignments is evaluated using simulated samples that were intentionally misaligned. This uncertainty is reported in Table 1.

To determine if a neutral meson oscillated into its antiparticle, knowledge of the B_s^0 or $\overline{B}_s^0$ flavour at production and decay is required. In $B_s^0 \to D_s^- \pi^+$ decays, the B_s^0 flavour at decay is identified by the charge of the pion as the $D_s^+ \pi^-$ decay cannot be directly produced. To determine whether the B_s^0 oscillated before decay, the flavour at production is inferred from the hadronization of the B_s^0 meson or the decay of other beauty hadrons produced in the collision using a combination of several flavour-tagging algorithms[34–37]. Each algorithm estimates the probability that a candidate has been assigned the wrong flavour tag. The algorithms that use information independent of signal fragmentation are calibrated using B^+ meson decays, and a combined wrong-tag estimate is used in the fit. The tagging efficiency is measured to be $\varepsilon = (80.30 \pm 0.07)\%$ with a probability to tag a candidate as the wrong flavour of $\omega = (36.21 \pm 0.17)\%$, where the uncertainties account for the calibration.

In the unbinned maximum likelihood fit to the decay time distribution used to extract Δm_s, the calibration parameters for the combined wrong-tag estimate are allowed to vary. Additional free parameters are the values of the spline coefficients used to describe the decay-time-dependent reconstruction efficiency and the B_s^0–$\overline{B}_s^0$ production and detection asymmetries.

The parameters Γ_s and $\Delta\Gamma_s$ are fixed in the fit to their known values[38]. The other fixed parameters are the estimate of the wrong-tag fraction and efficiency of the tagging algorithms, decay-time bias correction and decay-time resolution calibration parameters. The decay time distribution of the tagged–mixed ($\overline{B}_s^0 \to D_s^- \pi^+$), tagged–unmixed ($B_s^0 \to D_s^- \pi^+$) and untagged (where the initial flavour is unknown) samples are shown in Fig. 2 (left). The corresponding fit projection is overlaid. To highlight the oscillation phenomenon, the asymmetry distribution between the tagged–unmixed and tagged–mixed samples is defined as

$$A(t) = \frac{N(B_s^0 \to D_s^- \pi^+, t) - N(\overline{B}_s^0 \to D_s^- \pi^+, t)}{N(B_s^0 \to D_s^- \pi^+, t) + N(\overline{B}_s^0 \to D_s^- \pi^+, t)}, \qquad (2)$$

with t modulo $2\pi/\Delta m_s$, as shown in Fig. 2 (right). Here $N(\overline{B}_s^0 \to D_s^- \pi^+, t)$ and $N(B_s^0 \to D_s^- \pi^+, t)$ indicate the tagged–mixed and tagged–unmixed decays observed at time t, respectively. For this distribution, each event—in addition to the weight used to statistically subtract the background—is also weighted by the product of two factors. The first is a flavour-tagging dilution factor related to the probability that the flavour tag is indeed correct. The second is an effective decay-time uncertainty dilution factor depending on the reconstructed decay time per-event resolution and on Δm_s, for which the central value of the decay time fit is being used. The overlaid continuous line corresponds to the fit result. The result of the fit for Δm_s is $17.7683 \pm 0.0051\,\text{ps}^{-1}$, where this uncertainty is related to the sample size.

Several sources of systematic uncertainty have been investigated and those with a non-negligible contribution are listed in Table 1. These include uncertainty in the momentum scale of the detector, obtained by comparing the reconstructed masses of known particles with the most accurate available values[38]; residual detector misalignment and length-scale uncertainties; and uncertainties due to choice of mass and decay-time fit models, determined using alternate parameterizations and pseudo-experiments. To verify the robustness of the measurement to variations in Δm_s as a function of decay kinematics, the data sample is split into mutually disjoint subsamples, each having about the same number of signal events, in relevant kinematic quantities, such as the B_s^0 momentum, and the Δm_s values obtained from each subsample are compared. The largest observed variation is included as a systematic uncertainty. The total systematic uncertainty is $0.0032\,\text{ps}^{-1}$, with the leading

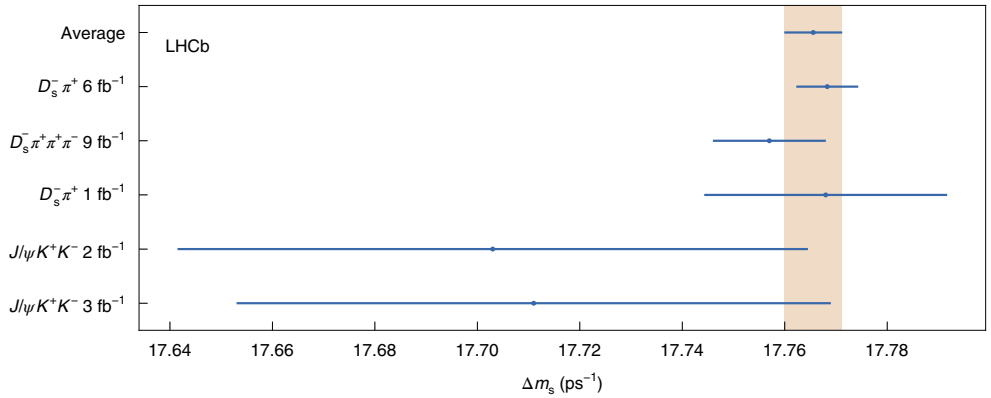

Fig. 3 | Summary of LHCb measurements. Comparison of LHCb Δm_s measurements obtained from refs. [9–12], the result presented in this article, and their average. The measurement described in this paper is labelled as $D_s^-\pi^+$ 6 fb^{-1}. The horizontal bars correspond to the total uncertainty reported for each measurement. The band indicates the size of the uncertainty on average for comparison purposes. The combination procedure and inputs are described in the text.

contribution due to residual detector misalignment and detector length-scale uncertainties.

The value of the B_s^0–$\overline{B}_s^0$ oscillation frequency determined in this article is as follows.

$$\Delta m_s = 17.7683 \pm 0.0051\,(\text{stat}) \pm 0.0032\,(\text{syst})\ \text{ps}^{-1}$$

This is the most precise measurement to date. The precision is further enhanced by combining this result with the values determined in refs. [9,12]. One study[9] used $B_s^0 \to D_s^-\pi^+$ decays collected in 2011. The other study[12] used a sample of $B_s^0 \to D_s^-\pi^+\pi^+\pi^-$ decays selected from the combined 2011–2018 dataset, corresponding to 9 fb^{-1}. The measurements are statistically independent. The systematic uncertainties related to the momentum scale, length scale and residual detector misalignment are assumed to be fully correlated. Due to aging of the detector and different alignment procedures used in Run 1 and Run 2, the effect of residual detector misalignment is larger in measurements using the Run 2 data. Given the precision of the measurement described in this paper, a detailed study of the detector misalignment effects is performed, and the related uncertainty due to the decay time bias has been substantially reduced compared with previous measurements using the Run 2 data. The values of the fixed parameters $\Delta\Gamma_s$ and Γ_s used as inputs to the previous analyses have evolved over time as additional measurements have been made. However, as the correlation between Δm_s and $\Delta\Gamma_s$ and Γ_s is negligible, these small differences have been ignored in the combination procedure. A covariance matrix is constructed by adding statistical and systematic uncertainties in quadrature for each input, including correlations between systematic uncertainties. The results are averaged by minimizing χ^2 from the full covariance matrix. The value of Δm_s obtained is $17.7666 \pm 0.0057\ \text{ps}^{-1}$. Additionally, these results are combined with those from refs. [10,11] where Δm_s is determined using $B_s^0 \to J/\psi K^+K^-$ decays in the 2011–2012 (3 fb^{-1}) and 2015–2016 (2 fb^{-1}) datasets. The decay time resolution for the measurements used in the combination[9–12], including the analysis presented here, varies from 35 to 45 fs, depending on the decay mode. The result for Δm_s is $17.7656 \pm 0.0057\ \text{ps}^{-1}$. The different measurements, as well as the resulting combination, are shown in Fig. 3.

In summary, this paper presents the most precise measurement of the Δm_s oscillation frequency, namely, $17.7683 \pm 0.0051\,(\text{stat}) \pm 0.0032\,(\text{syst})\ \text{ps}^{-1}$, where the first uncertainty is statistical and the second is systematic. The result is obtained using a sample of $B_s^0 \to D_s^-\pi^+$ decays collected with the LHCb detector during Run 2 of the LHC. Combining the result of this paper with previous measurements by the LHCb collaboration yields $\Delta m_s = 17.7656 \pm 0.0057\ \text{ps}^{-1}$. This value is compatible with, and considerably more precise than, the predicted value from lattice quantum chromodynamics (refs. [13–15]) and sum-rule calculations[16,17] of $18.4^{+0.7}_{-1.2}\ \text{ps}^{-1}$ (ref. [18]). The combined result represents a considerable improvement over previous measurements, and is a legacy measurement of the original LHCb detector. The experiment is currently undergoing a major upgrade to operate at five times the instantaneous luminosity from 2022 onwards[39]. The largest sources of systematic uncertainty for this measurement, that is, those related to the detector length scale and misalignment, will be a focal point to further improve on this result for future data-taking periods.

Online content

Any methods, additional references, Nature Research reporting summaries, source data, extended data, supplementary information, acknowledgements, peer review information; details of author contributions and competing interests; and statements of data and code availability are available at https://doi.org/10.1038/s41567-021-01394-x.

Received: 12 April 2021; Accepted: 17 September 2021;
Published online: 6 January 2022

References

1. Lenz, A. & Nierste, U. Theoretical update of B_s^0–$\bar{B}_s^0$ mixing. *J. High Energ. Phys.* **06**, 072 (2007).
2. Cabibbo, N. Unitary symmetry and leptonic decays. *Phys. Rev. Lett.* **10**, 531–533 (1963).
3. Kobayashi, M. & Maskawa, T. CP-violation in the renormalizable theory of weak interaction. *Prog. Theor. Phys.* **49**, 652–657 (1973).
4. UTfit collaboration et al. The unitarity triangle fit in the standard model and hadronic parameters from lattice QCD: a reappraisal after the measurements of Δm_s and $BR(B\to\tau\nu_\tau)$. *J. High Energ. Phys.* **10**, 081 (2006).
5. The CKMfitter Group Current status of the standard model CKM fit and constraints on $\Delta F=2$ new physics. *Phys. Rev.* **D91**, 073007 (2015).
6. Aoki, S. et al. FLAG review 2019. *Eur. Phys. J. C* **80**, 113 (2020).
7. The LHCb collaboration et al. Measurement of CP asymmetry in $B_s^0 \to D_s^{\mp}K^{\pm}$ decays. *J. High Energ. Phys.* **2018**, 059 (2018).
8. CDF collaboration Observation of B_s^0–$\bar{B}_s^0$ oscillations. *Phys. Rev. Lett.* **97**, 242003 (2006).
9. LHCb collaboration et al. Precision measurement of the B_s^0–B_s^0 oscillation frequency in the decay B_s^0. *New J. Phys.* **15**, 053021 (2013).
10. LHCb collaboration et al. Precision measurement of CP violation in $B_s^0 \to J/\psi K^+K^-$. *Phys. Rev. Lett.* **114**, 041801 (2015).
11. LHCb collaboration et al. Updated measurement of time-dependent CP-violating observables in $B_s^0 \to J/\psi K^+K^-$ decays. *Eur. Phys. J. C* **79**, 706 (2019); erratum **80**, 601 (2020).
12. LHCb collaboration et al. Measurement of the CKM angle γ and B_s^0–B_s^0 mixing frequency with B_s^0 decays. *J. High Energ. Phys.* **03**, 137 (2021).

13. Bazavov, A. et al. $B^0_{(s)}$-mixing matrix elements from lattice QCD for the standard model and beyond. *Phys. Rev. D* **93**, 113016 (2016).
14. RBC/UKQCD collaboration. SU(3)-breaking ratios for $D_{(s)}$ and $B_{(s)}$ mesons. Preprint at https://arxiv.org/abs/1812.08791 (2018).
15. Dowdall, R. J. et al. Neutral *B*-meson mixing from full lattice QCD at the physical point. *Phys. Rev. D* **100**, 094508 (2019).
16. Grozin, A. G., Thomas, T. & Pivovarov, A. A. $B^0-\overline{B}^0$ mixing: matching to HQET at NNLO. *Phys. Rev. D* **98**, 054020 (2018).
17. King, D., Lenz, A. & Rauh, T. B^0_s mixing observables and V_{td}/V_{ts} from sum rules. *J. High Energ. Phys.* **05**, 034 (2019).
18. Di Luzio, L., Kirk, M., Lenz, A. & Rauh, T. ΔM_s theory precision confronts flavour anomalies. *J. High Energ. Phys.* **2019**, 9 (2019).
19. LHCb collaboration et al. The LHCb detector at the LHC. *JINST* **3**, S08005 (2008).
20. LHCb collaboration et al. LHCb detector performance. *Int. J. Mod. Phys.* **A30**, 1530022 (2015).
21. Sjöstrand, T., Mrenna, S. & Skands, P. A brief introduction to PYTHIA 8.1. *Comput. Phys. Commun.* **178**, 852–867 (2008).
22. Belyaev, I. et al. Handling of the generation of primary events in Gauss, the LHCb simulation framework. *J. Phys. Conf. Ser.* **331**, 032047 (2011).
23. Lange, D. J. The EvtGen particle decay simulation package. *Nucl. Instrum. Meth.* **A462**, 152–155 (2001).
24. Geant4 collaboration et al. Geant4 developments and applications. *IEEE Trans. Nucl. Sci.* **53**, 270–278 (2006).
25. Geant4 collaboration et al. Geant4: a simulation toolkit. *Nucl. Instrum. Meth.* **A506**, 250–303 (2003).
26. Clemencic, M. et al. The LHCb simulation application, Gauss: design, evolution and experience. *J. Phys. Conf. Ser.* **331**, 032023 (2011).
27. Davidson, N., Przedzinski, T. & Was, Z. PHOTOS interface in C++: technical and physics documentation. *Comp. Phys. Comm.* **199**, 86–101 (2016).
28. Aaij, R. et al. Performance of the LHCb trigger and full real-time reconstruction in Run 2 of the LHC. *JINST* **14**, P04013 (2019).
29. Pivk, M. & Le Diberder, F. R. sPlot: a statistical tool to unfold data distributions. *Nucl. Instrum. Meth.* **A555**, 356–369 (2005).
30. Martínez Santos, D. & Dupertuis, F. Mass distributions marginalized over per-event errors. *Nucl. Instrum. Meth.* **A764**, 150–155 (2014).
31. Johnson, L. N. Systems of frequency curves generated by methods of translation. *Biometrika* **36**, 149–176 (1949).
32. LHCb collaboration et al. Measurement of B^0, B^0_s, B^+ and Λ^0_b production asymmetries in 7 and 8 TeV proton–proton collisions. *Phys. Lett. B* **774**, 139–158 (2017).
33. Karbach, T. M., Raven, G. & Schiller, M. Decay time integrals in neutral meson mixing and their efficient evaluation. Preprint at https://arxiv.org/abs/1407.0748 (2014).
34. Fazzini, D., Flavour tagging in the LHCb experiment. In *Proc. Sixth Annual Conference on Large Hadron Collider Physics, Bologna, Italy, 4–9 June 2018* 230 (PoS, 2018).
35. LHCb collaboration et al. Opposite-side flavour tagging of *B* mesons at the LHCb experiment. *Eur. Phys. J. C* **72**, 2022 (2012).
36. LHCb collaboration et al. *B* flavour tagging using charm decays at the LHCb experiment. *JINST* **10**, P10005 (2015).
37. LHCb collaboration et al. A new algorithm for identifying the flavour of B^0_s mesons at LHCb. *JINST* **11**, P05010 (2016).
38. Particle Data Group et al. Review of particle physics. *Prog. Theor. Exp. Phys.* **2020**, 083C01 (2020).
39. LHCb collaboration et al. Framework TDR for the LHCb upgrade: technical design report. CERN-LHCC-2012-007 (2012).

Methods

The LHCb detector. The LHCb detector[19,20] is a single-arm forward spectrometer covering the pseudo-rapidity range of $2<\eta<5$, designed for the study of particles containing b or c quarks. The detector includes a high-precision tracking system consisting of a silicon-strip vertex detector surrounding the pp interaction region[40], a large-area silicon-strip detector located upstream of a dipole magnet with a bending power of about 4 T m, and three stations of silicon-strip detectors and straw drift tubes[41] placed downstream of the magnet. The tracking system provides a measurement of momentum p of the charged particles with a relative uncertainty that varies from 0.5% at low momentum to 1.0% at 200 GeV c^{-1}. The minimum distance of a track to a primary vertex (PV), that is, the impact parameter, is measured with a resolution of $(15+29/p_{\rm T})\,\mu$m, where $p_{\rm T}$ is the component of the momentum transverse to the beam (unit, GeV c^{-1}). Different types of charged hadron are distinguished using information from two ring-imaging Cherenkov detectors[42]. Photons, electrons and hadrons are identified by a calorimeter system consisting of scintillating-pad and preshower detectors and an electromagnetic and hadronic calorimeter. Muons are identified by a system composed of alternating layers of iron and multiwire proportional chambers[43].

Simulation of the LHCb detector response is required to model the effects of detector acceptance and imposed selection requirements. In the simulation, pp collisions are generated using PYTHIA[21] with a specific LHCb configuration[22]. Decays of unstable particles are described by EvtGen[23], in which the final-state radiation is generated using PHOTOS[27]. The interaction of the generated particles with the detector and its response are implemented using the GEANT4 toolkit[24,25] described in ref. [26].

Selection. A fast decision about which pp collisions are of interest is made by a trigger system[44]. It consists of a hardware stage, based on information from the calorimeter and muon systems, followed by a software stage that reconstructs the pp collision based on all the available detector information. The software trigger selects candidates consistent with a b-hadron decay topology, with tracks originating from a vertex detached from the primary pp collision point, known as the PV. The mean B_s^0 lifetime is 1.5 ps (ref. [38]), which corresponds to an average flight distance of 1 cm in the LHCb detector.

After being accepted by the trigger, a further selection is applied that forms $D_s^-\to {\rm K}^-{\rm K}^+\pi^-$ and $D_s^-\to\pi^-\pi^+\pi^-$ candidates from the reconstructed charged tracks and subsequently combines them with a fourth track to form $B_s^0\to D_s^-\pi^+$ candidates. Particle identification information is used to assign mass hypotheses to each of the final-state tracks.

The B_s^0 invariant mass resolution is improved by constraining the D_s^- invariant mass to its known value[38]. The $K^+K^-\pi^\pm$ or $\pi^+\pi^-\pi^\pm$ and $D_s^-\pi^+$ invariant mass ranges considered in this analysis are [1,930, 2,015] and [5,300, 5,800] MeV c^{-2}, respectively.

To suppress the B_s^0 candidates formed from random track combinations, a gradient boosted decision tree (BDT) is used, implemented using the XGBoost library[45]. Training uses data from both signal and background samples to avoid mismatches between the data and simulation. This classifier uses information on the fit quality of the D_s^- and B_s^0 decay vertices; D_s^- and $B_s^0\,\chi^2_{\rm IP}$ defined as the difference in χ^2 of the vertex fit for a given PV reconstructed with and without the considered particle; angles between their momentum vector and vector connecting their production and decay vertices; and $p_{\rm T}$ and impact parameter $\chi^2_{\rm IP}$ of the final-state tracks. The BDT classifier threshold is chosen to maximize the product of the signal significance and signal efficiency. This choice optimizes sensitivity to the oscillation frequency.

Flavour tagging. The initial flavour of the B_s^0 meson must be known to determine if it has oscillated before decay. Flavour-tagging algorithms are used to determine the initial flavour from properties of the b-hadron production in the pp collision.

Beauty quarks are predominantly produced in pairs. Opposite-side (OS) tagging algorithms[35] determine the initial flavour of the B_s^0 meson based on information from the other beauty quark decay. These include the OS muon and OS electron taggers, which identify the flavour from the charge of leptons produced in the other b-hadron decay. The OS kaon tagger identifies $b\to c\to s$ transitions, the OS charm quark tagger identifies $b\to c$ transitions, and the OS vertex charge tagger calculates the effective charge of an OS displaced vertex[36]. In addition, a same-side kaon tagger exploits the charge information of the kaon originating from the $\bar{s}$ or s quark leftover from the B_s^0 or $\overline{B}{}_s^0$ meson fragmentation[37]. Each algorithm determines the initial flavour of the B_s^0 meson from the charge of the reconstructed tagging particle or the reconstructed vertex in case of the OS vertex tagger.

The tagging information is incorporated in the decay time description. The amplitude of oscillation is reduced by a dilution factor $D=(1-2\omega)$, where ω is the average fraction of incorrect tags (known as mistag rate in the literature). Different machine-learning algorithms provide an estimate of the mistag rate that is calibrated with the data to match the true mistag distribution. A linear calibration of the average mistag as a function of the predicted mistag for the combined OS tag and same-side kaon tag information is then implemented in the decay time fit with freely varying calibration parameters. The combined tagging efficiency of the sample is $\varepsilon=(80.30\pm0.07)\%$ with a mistag fraction of $\omega=(36.21\pm0.02\pm0.17)\%$, where the first uncertainty is due to the finite size of the calibration sample and the second one is due to the calibration procedure. This results in a combined effective performance of $(6.10\pm0.02\pm0.15)\%$ with respect to a perfect tagging algorithm that would have 100% tagging efficiency and zero mistag rate.

Decay time fit. The observed decay time distribution is fitted using an unbinned maximum likelihood fit in which all the combinations of initial-state flavours (B_s^0, $\overline{B}{}_s^0$ or untagged) and final-state charges ($D_s^-\pi^+$ or $D_s^+\pi^-$) are simultaneously fit. The decay time distribution of each measured final state is described by the sum of all the processes contributing to that state. Experimental effects are taken into account with several adjustments to the theoretical prediction in equation (1), namely,

$$P_{\rm exp}(B_s^0\to D_s^-\pi^+,t)\approx(1+a_{\rm det})\left[(1-\omega)(1-a_{\rm prod})P(B_s^0\to D_s^-\pi^+,t)+\omega(1+a_{\rm prod})P(\overline{B}{}_s^0\to D_s^-\pi^+,t)\right]. \quad (3)$$

Production and detection asymmetries are parameterized by factors $a_{\rm prod}$ and $a_{\rm det}$, respectively, which are allowed to deviate from unity. The decay time distribution of both flavours contain a fraction $(1-\omega)$ of the correctly tagged decay time parameterization plus a fraction ω of the incorrectly tagged decay time parameterization. The mistag rate ω is obtained from a per-event estimation, after linear calibration. Different calibration parameters are used for the B_s^0 and $\overline{B}{}_s^0$ initial flavours.

The experimental decay time distributions of both flavours are convolved with a Gaussian function to account for the finite detector resolution. The mean of this function is shifted by the decay-time bias correction factor, and the width is obtained from a per-event estimate of the decay time uncertainty after linear calibration.

A decay-time-dependent efficiency is finally modelled by a time-dependent cubic spline function, which multiplies the decay time distribution obtained from the previous step.

Systematic uncertainties. The following sources of systematic uncertainty have been found to give a non-negligible contribution to the Δm_s measurement. These are summarized in Table 1.

The measured decay time is inversely proportional to B_s^0 momentum and therefore depends on an accurate determination of the momentum-scale uncertainty of the tracking system. The uncertainty is determined by varying the momentum of the B_s^0 meson by $\pm0.03\%$ (obtained from a comparison of masses of different particles with their known values) in the simulated signal samples. The corresponding uncertainty in Δm_s is 0.0007 ps^{-1}.

The measured decay time is also proportional to the distance travelled by the B_s^0 meson between production and decay, which is affected by the precise knowledge of the position of the vertex detector elements along the proton beam axis. The measured uncertainty is 100 µm over a length of 1 m (ref. [40]). The corresponding uncertainty in Δm_s is 0.0018 ps^{-1}.

The relative alignment of the tracking detector elements is a source of bias in decay time and contributes to resolution effects. The uncertainty in Δm_s due to imprecise knowledge of this alignment has been obtained from the analysis of the simulated signal samples in which the detector elements have been deliberately misaligned. Different misalignments, namely, translations, rotations and their combinations—have been investigated. The leading effect is due to translation along the x axis—the axis perpendicular to the beam direction pointing towards the centre of the LHC ring. As a consequence, the simulated signal samples have been misaligned with x-axis translations in the range between 0 and 9 µm, as determined from the survey results. Each misaligned simulated sample is then corrected for decay time bias in the same manner as the data, and the extracted Δm_s value is compared with the value obtained in simulation without any misalignment. This comparison produces a corresponding uncertainty in the bias correction procedure of 0.0020 ps^{-1}.

Alternative parameterizations of the background contributions to the invariant mass fit have been obtained by using different weighting methods; the difference between these parameterizations corresponds to an uncertainty of 0.0002 ps^{-1}.

For the specific $B_s^0\to D_s^{*-}\pi^+$ and $B^0\to D_s^-\pi^+$ background contributions, the relative fraction of these components cannot be reliably determined from the data. Their relative contributions are nominally set to an equal mixture and varied between 0 (pure $B^0\to D_s^-\pi^+$) and 1 (pure $B_s^0\to D_s^{*-}\pi^+$) to determine the maximum deviation in Δm_s corresponding to an uncertainty of 0.0005 ps^{-1}.

The decay time resolution is obtained from data using a sample of D_s^- mesons that are directly produced in a pp collision. These are combined with a π^+ meson coming from the same collision to produce a fake B_s^0 candidate with a decay time equal to zero, ignoring the resolution effects. Different parameterizations of the measured decay time distribution are applied to a simulated signal sample. The largest deviation of the extracted Δm_s value with respect to nominal parameterization is found to be 0.0011 ps^{-1}.

The procedure used to subtract background contributions in the fit to the decay time distribution assumes no large correlations between the decay time and the reconstructed B_s^0 and D_s^- invariant masses. This is studied by analysing the

simulated signal and background samples where any residual correlations between these observables are removed. The difference in measured value of Δm_s between the decorrelated and nominal samples is found to be 0.0011 ps^{-1}.

The data sample was split into mutually disjoint subsamples to study the effect of potential correlations between the kinematic ranges, data-taking periods, flavour-tagging categories, BDT-based selection and measured value of Δm_s. The measured values obtained from each subsample are compared and the largest observed variation is found to be 0.0003 ps^{-1}.

Several additional effects have been considered consisting of possible biases introduced by the fit procedure, changes to the signal and background parameterizations, and changes in the reweighting procedure used when obtaining the invariant mass shapes of partially reconstructed backgrounds constituting less than 2% of the signal yield. Their impact has been found to be negligible with respect to the sources listed in Table 1.

The largest sources of systematic uncertainty are found to be due to the imprecise knowledge of position and alignment of the tracking detector closest to the nominal pp collision region.

Data availability

All figures are available at https://lhcbproject.web.cern.ch/Publications/p/LHCb-PAPER-2021-005.html. Additional material describing this analysis is available at http://cds.cern.ch/record/2764338/files/ in the 'Supplementary.pdf' file in 'LHCb-PAPER-2021-005-supplementary.zip'. Inputs to the Δm_s combination are available from the HEP data at https://www.hepdata.net/record/105881. LHCb has an open data policy described in http://cdsweb.cern.ch/record/1543410. Subject to the resources being identified, LHCb will endeavour to provide open access to some reconstructed level data on the disk at CERN.

Code availability

The code used for the fit to the B_s^0 and D_s^- invariant mass distributions and to the B_s^0 decay time distribution is publicly available at https://gitlab.cern.ch/lhcb/Urania/-/tree/master/PhysFit/B2DXFitters.

References

40. Aaij, R. et al. Performance of the LHCb vertex locator. *JINST* **9**, P09007 (2014).
41. d'Argent, P. et al. Improved performance of the LHCb outer tracker in LHC Run 2. *JINST* **12**, P11016 (2017).
42. Adinolfi, M. et al. Performance of the LHCb RICH detector at the LHC. *Eur. Phys. J. C* **73**, 2431 (2013).
43. Alves, A. A. Performance of the LHCb muon system. *JINST* **8**, P02022 (2013).
44. Aaij, R. et al. The LHCb trigger and its performance in 2011. *JINST* **8**, P04022 (2013).
45. Chen, T. & Guestrin, C. XGBoost: a scalable tree boosting system. In *KDD '16: Proc. 22nd ACM SIGKDD International Conference on Knowledge Discovery and Data Mining (NY, USA)* 785–794 (ACM, 2016).

Acknowledgements

We thank our colleagues in the CERN accelerator departments for the excellent performance of the LHC. We thank the technical and administrative staff at the LHCb institutes. We acknowledge support from CERN and from the following national agencies: CAPES, CNPq, FAPERJ and FINEP (Brazil); MOST and NSFC (China); CNRS/IN2P3 (France); BMBF, DFG and MPG (Germany); INFN (Italy); NWO (Netherlands); MNiSW and NCN (Poland); MEN/IFA (Romania); MSHE (Russia); MICINN (Spain); SNSF and SER (Switzerland); NASU (Ukraine); STFC (UK); DOE NP and NSF (USA). We acknowledge the computing resources that are provided by CERN, IN2P3 (France), KIT and DESY (Germany), INFN (Italy), SURF (Netherlands), PIC (Spain), GridPP (UK), RRCKI and Yandex LLC (Russia), CSCS (Switzerland), IFIN-HH (Romania), CBPF (Brazil), PL-GRID (Poland) and NERSC (USA). We are indebted to the communities behind the multiple open-source software packages on which we depend. Individual groups or members have received support from ARC and ARDC (Australia); AvH Foundation (Germany); EPLANET, Marie Skłodowska-Curie Actions and ERC (European Union); A*MIDEX, ANR, Labex P2IO and OCEVU, and Région Auvergne-Rhône-Alpes (France); Key Research Program of Frontier Sciences of CAS, CAS PIFI, CAS CCEPP, Fundamental Research Funds for the Central Universities, and Sci. & Tech. Program of Guangzhou (China); RFBR, RSF and Yandex LLC (Russia); GVA, XuntaGal and GENCAT (Spain); the Leverhulme Trust, the Royal Society and UKRI (UK).

Author contributions

All authors have contributed to the publication, being variously involved in the design and the construction of detectors, in writing software, in operating the detectors and acquiring data, in calibrating the sub-systems and processing data, and finally in analysing the processed data.

Competing interests

The authors declare no competing interests.

Additional information

Correspondence and requests for materials should be addressed to A. Bertolin.

Peer review information *Nature Physics* thanks Joseph Kroll, Alexander Lenz and the other, anonymous, reviewer(s) for their contribution to the peer review of this work.

Reprints and permissions information is available at www.nature.com/reprints.

LHCb collaboration

R. Aaij[1], C. Abellán Beteta[2], T. Ackernley[3], B. Adeva[4], M. Adinolfi[5], H. Afsharnia[6], C. A. Aidala[7], S. Aiola[8], Z. Ajaltouni[6], S. Akar[9], J. Albrecht[10], F. Alessio[11], M. Alexander[12], A. Alfonso Albero[13], Z. Aliouche[14], G. Alkhazov[15], P. Alvarez Cartelle[16], S. Amato[17], Y. Amhis[18], L. An[11], L. Anderlini[19], A. Andreianov[15], M. Andreotti[20], F. Archilli[21], A. Artamonov[22], M. Artuso[23], K. Arzymatov[24], E. Aslanides[25], M. Atzeni[2], B. Audurier[26], S. Bachmann[21], M. Bachmayer[27], J. J. Back[28], P. Baladron Rodriguez[4], V. Balagura[26], W. Baldini[20], J. Baptista Leite[29], R. J. Barlow[14], S. Barsuk[18], W. Barter[30], M. Bartolini[31], F. Baryshnikov[32], J. M. Basels[33], G. Bassi[34], B. Batsukh[23], A. Battig[10], A. Bay[27], M. Becker[10], F. Bedeschi[34], I. Bediaga[29], A. Beiter[23], V. Belavin[24], S. Belin[35], V. Bellee[27], K. Belous[22], I. Belov[36], I. Belyaev[37], G. Bencivenni[38], E. Ben-Haim[39], A. Berezhnoy[36], R. Bernet[2], D. Berninghoff[21], H. C. Bernstein[23], C. Bertella[11], A. Bertolin[40] ✉, C. Betancourt[2], F. Betti[11], Ia. Bezshyiko[2], S. Bhasin[5], J. Bhom[41], L. Bian[42], M. S. Bieker[10], S. Bifani[43], P. Billoir[39], M. Birch[30], F. C. R. Bishop[16], A. Bitadze[14], A. Bizzeti[19,44], M. Bjørn[45], M. P. Blago[11], T. Blake[28], F. Blanc[27], S. Blusk[23], D. Bobulska[12], J. A. Boelhauve[10], O. Boente Garcia[4], T. Boettcher[46], A. Boldyrev[47], A. Bondar[48], N. Bondar[11,15], S. Borghi[14], M. Borisyak[24], M. Borsato[21], J. T. Borsuk[41], S. A. Bouchiba[27], T. J. V. Bowcock[3], A. Boyer[11], C. Bozzi[20], M. J. Bradley[30], S. Braun[49], A. Brea Rodriguez[4], M. Brodski[11], J. Brodzicka[41], A. Brossa Gonzalo[28], D. Brundu[35], A. Buonaura[2], C. Burr[11], A. Bursche[50], A. Butkevich[51], J. S. Butter[1], J. Buytaert[11], W. Byczynski[11], S. Cadeddu[35], H. Cai[42], R. Calabrese[20,52], L. Calefice[10,39], L. Calero Diaz[38], S. Cali[38], R. Calladine[43], M. Calvi[53,54], M. Calvo Gomez[55], P. Camargo Magalhaes[5], A. Camboni[13,55], P. Campana[38], A. F. Campoverde Quezada[56], S. Capelli[53,54], L. Capriotti[57,58], A. Carbone[57,58], G. Carboni[59], R. Cardinale[31], A. Cardini[35], I. Carli[60], P. Carniti[53,54], L. Carus[33], K. Carvalho Akiba[1], A. Casais Vidal[4], G. Casse[3], M. Cattaneo[11], G. Cavallero[11], S. Celani[27], J. Cerasoli[25], A. J. Chadwick[3], M. G. Chapman[5], M. Charles[39], Ph. Charpentier[11], G. Chatzikonstantinidis[43], C. A. Chavez Barajas[3], M. Chefdeville[61], C. Chen[62], S. Chen[60], A. Chernov[41], V. Chobanova[4], S. Cholak[27], M. Chrzaszcz[41], A. Chubykin[15], V. Chulikov[15], P. Ciambrone[38], M. F. Cicala[28], X. Cid Vidal[4], G. Ciezarek[11], P. E. L. Clarke[63], M. Clemencic[11], H. V. Cliff[16], J. Closier[11], J. L. Cobbledick[14], V. Coco[11], J. A. B. Coelho[18], J. Cogan[25], E. Cogneras[6], L. Cojocariu[64], P. Collins[11], T. Colombo[11], L. Congedo[65,66], A. Contu[35], N. Cooke[43], G. Coombs[12], G. Corti[11], C. M. Costa Sobral[28], B. Couturier[11], D. C. Craik[46], J. Crkovská[67], M. Cruz Torres[29], R. Currie[63], C. L. Da Silva[67], E. Dall'Occo[10], J. Dalseno[4], C. D'Ambrosio[11], A. Danilina[37], P. d'Argent[11], A. Davis[14], O. De Aguiar Francisco[14], K. De Bruyn[68], S. De Capua[14], M. De Cian[27], J. M. De Miranda[29], L. De Paula[17], M. De Serio[65,66], D. De Simone[2], P. De Simone[38], J. A. de Vries[69], C. T. Dean[67], D. Decamp[61], L. Del Buono[39], B. Delaney[16], H.-P. Dembinski[10], A. Dendek[70], V. Denysenko[2], D. Derkach[47], O. Deschamps[6], F. Desse[18], F. Dettori[35,71], B. Dey[72], P. Di Nezza[38], S. Didenko[32], L. Dieste Maronas[4], H. Dijkstra[11], V. Dobishuk[73], A. M. Donohoe[74], F. Dordei[35], A. C. dos Reis[29], L. Douglas[12], A. Dovbnya[75], A. G. Downes[61], K. Dreimanis[3], M. W. Dudek[41], L. Dufour[11], V. Duk[76], P. Durante[11], J. M. Durham[67], D. Dutta[14], A. Dziurda[41], A. Dzyuba[15], S. Easo[77], U. Egede[78], V. Egorychev[37], S. Eidelman[48,79], S. Eisenhardt[63], S. Ek-In[27], L. Eklund[12,80], S. Ely[23], A. Ene[64], E. Epple[67], S. Escher[33], J. Eschle[2], S. Esen[39], T. Evans[11], A. Falabella[57], J. Fan[62], Y. Fan[56], B. Fang[42], S. Farry[3], D. Fazzini[53,54], M. Féo[11], A. Fernandez Prieto[4], J. M. Fernandez-tenllado Arribas[13], A. D. Fernez[49], F. Ferrari[57,58], L. Ferreira Lopes[27], F. Ferreira Rodrigues[17], S. Ferreres Sole[1], M. Ferrillo[2], M. Ferro-Luzzi[11], S. Filippov[51], R. A. Fini[65], M. Fiorini[20,52], M. Firlej[70], K. M. Fischer[45], D. S. Fitzgerald[7], C. Fitzpatrick[14], T. Fiutowski[70], F. Fleuret[26], M. Fontana[39], F. Fontanelli[31,81], R. Forty[11], V. Franco Lima[3], M. Franco Sevilla[49], M. Frank[11],

E. Franzoso[20], G. Frau[21], C. Frei[11], D. A. Friday[12], J. Fu[8], Q. Fuehring[10], W. Funk[11], E. Gabriel[1], T. Gaintseva[24], A. Gallas Torreira[4], D. Galli[57,58], S. Gambetta[11,63], Y. Gan[62], M. Gandelman[17], P. Gandini[8], Y. Gao[82], M. Garau[35], L. M. Garcia Martin[28], P. Garcia Moreno[13], J. García Pardiñas[53,54], B. Garcia Plana[4], F. A. Garcia Rosales[26], L. Garrido[13], C. Gaspar[11], R. E. Geertsema[1], D. Gerick[21], L. L. Gerken[10], E. Gersabeck[14], M. Gersabeck[14], T. Gershon[28], D. Gerstel[25], Ph. Ghez[61], V. Gibson[16], H. K. Giemza[83], M. Giovannetti[38,84], A. Gioventù[4], P. Gironella Gironell[13], L. Giubega[64], C. Giugliano[11,20,71], K. Gizdov[63], E. L. Gkougkousis[11], V. V. Gligorov[39], C. Göbel[85], E. Golobardes[55], D. Golubkov[37], A. Golutvin[30,32], A. Gomes[29,86], S. Gomez Fernandez[13], F. Goncalves Abrantes[45], M. Goncerz[41], G. Gong[62], P. Gorbounov[37], I. V. Gorelov[36], C. Gotti[53], E. Govorkova[11], J. P. Grabowski[21], T. Grammatico[39], L. A. Granado Cardoso[11], E. Graugés[13], E. Graverini[27], G. Graziani[19], A. Grecu[64], L. M. Greeven[1], P. Griffith[20,52], L. Grillo[14], S. Gromov[32], B. R. Gruberg Cazon[45], C. Gu[62], M. Guarise[20], P. A. Günther[21], E. Gushchin[51], A. Guth[33], Y. Guz[22], T. Gys[11], T. Hadavizadeh[78], G. Haefeli[27], C. Haen[11], J. Haimberger[11], T. Halewood-leagas[3], P. M. Hamilton[49], J. P. Hammerich[3], Q. Han[87], X. Han[21], T. H. Hancock[45], S. Hansmann-Menzemer[21], N. Harnew[45], T. Harrison[3], C. Hasse[11], M. Hatch[11], J. He[56,88], M. Hecker[30], K. Heijhoff[1], K. Heinicke[10], A. M. Hennequin[11], K. Hennessy[3], L. Henry[8,89], J. Heuel[33], A. Hicheur[17], D. Hill[27], M. Hilton[14], S. E. Hollitt[10], J. Hu[21], J. Hu[50], W. Hu[87], W. Huang[56], X. Huang[42], W. Hulsbergen[1], R. J. Hunter[28], M. Hushchyn[47], D. Hutchcroft[3], D. Hynds[1], P. Ibis[10], M. Idzik[70], D. Ilin[15], P. Ilten[9], A. Inglessi[15], A. Ishteev[32], K. Ivshin[15], R. Jacobsson[11], S. Jakobsen[11], E. Jans[1], B. K. Jashal[89], A. Jawahery[49], V. Jevtic[10], M. Jezabek[41], F. Jiang[62], M. John[45], D. Johnson[11], C. R. Jones[16], T. P. Jones[28], B. Jost[11], N. Jurik[11], S. Kandybei[75], Y. Kang[62], M. Karacson[11], M. Karpov[47], F. Keizer[11], M. Kenzie[28], T. Ketel[90], B. Khanji[10], A. Kharisova[91], S. Kholodenko[22], T. Kirn[33], V. S. Kirsebom[27], O. Kitouni[46], S. Klaver[1], K. Klimaszewski[83], S. Koliiev[73], A. Kondybayeva[32], A. Konoplyannikov[37], P. Kopciewicz[70], R. Kopecna[21], P. Koppenburg[1], M. Korolev[36], I. Kostiuk[1,73], O. Kot[73], S. Kotriakhova[15,20], P. Kravchenko[15], L. Kravchuk[51], R. D. Krawczyk[11], M. Kreps[28], F. Kress[30], S. Kretzschmar[33], P. Krokovny[48,79], W. Krupa[70], W. Krzemien[83], W. Kucewicz[41,92], M. Kucharczyk[41], V. Kudryavtsev[48,79], H. S. Kuindersma[1,90], G. J. Kunde[67], T. Kvaratskheliya[37], D. Lacarrere[11], G. Lafferty[14], A. Lai[35], A. Lampis[35], D. Lancierini[2], J. J. Lane[14], R. Lane[5], G. Lanfranchi[38], C. Langenbruch[33], J. Langer[10], O. Lantwin[2], T. Latham[28], F. Lazzari[34,93], R. Le Gac[25], S. H. Lee[7], R. Lefèvre[6], A. Leflat[36], S. Legotin[32], O. Leroy[25], T. Lesiak[41], B. Leverington[21], H. Li[50], L. Li[45], P. Li[21], S. Li[87], Y. Li[60], Y. Li[60], Z. Li[23], X. Liang[23], T. Lin[30], R. Lindner[11], V. Lisovskyi[10], R. Litvinov[35], G. Liu[50], H. Liu[56], S. Liu[60], X. Liu[62], A. Loi[35], J. Lomba Castro[4], I. Longstaff[12], J. H. Lopes[17], G. H. Lovell[16], Y. Lu[60], D. Lucchesi[40,94], S. Luchuk[51], M. Lucio Martinez[1], V. Lukashenko[1], Y. Luo[62], A. Lupato[14], E. Luppi[20,52], O. Lupton[28], A. Lusiani[34,95], X. Lyu[56], L. Ma[60], R. Ma[56], S. Maccolini[57,58], F. Machefert[18], F. Maciuc[64], V. Macko[27], P. Mackowiak[10], S. Maddrell-Mander[5], O. Madejczyk[70], L. R. Madhan Mohan[5], O. Maev[15], A. Maevskiy[47], D. Maisuzenko[15], M. W. Majewski[70], J. J. Malczewski[41], S. Malde[45], B. Malecki[11], A. Malinin[96], T. Maltsev[48,79], H. Malygina[21], G. Manca[35,71], G. Mancinelli[25], D. Manuzzi[57,58], D. Marangotto[8,97], J. Maratas[6,98], J. F. Marchand[61], U. Marconi[57], S. Mariani[19,99], C. Marin Benito[11], M. Marinangeli[27], J. Marks[21], A. M. Marshall[5], P. J. Marshall[3], G. Martellotti[100], L. Martinazzoli[11,54], M. Martinelli[53,54], D. Martinez Santos[4], F. Martinez Vidal[89], A. Massafferri[29], M. Materok[33], R. Matev[11], A. Mathad[2], Z. Mathe[11], V. Matiunin[37], C. Matteuzzi[53], K. R. Mattioli[7], A. Mauri[1], E. Maurice[26], J. Mauricio[13], M. Mazurek[11], M. McCann[30], L. Mcconnell[74], T. H. Mcgrath[14], A. McNab[14], R. McNulty[74], J. V. Mead[3], B. Meadows[9], C. Meaux[25], G. Meier[10], N. Meinert[101], D. Melnychuk[83], S. Meloni[53,54], M. Merk[1,69], A. Merli[8], L. Meyer Garcia[17], M. Mikhasenko[11], D. A. Milanes[102], E. Millard[28], M. Milovanovic[11],

M.-N. Minard[61], A. Minotti[20], L. Minzoni[20,52], S. E. Mitchell[63], B. Mitreska[14], D. S. Mitzel[11], A. Mödden[10], R. A. Mohammed[45], R. D. Moise[30], T. Mombächer[10], I. A. Monroy[102], S. Monteil[6], M. Morandin[40], G. Morello[38], M. J. Morello[34,95], J. Moron[70], A. B. Morris[103], A. G. Morris[28], R. Mountain[23], H. Mu[62], F. Muheim[11,63], M. Mulder[11], D. Müller[11], K. Müller[2], C. H. Murphy[45], D. Murray[14], P. Muzzetto[11,35], P. Naik[5], T. Nakada[27], R. Nandakumar[77], T. Nanut[27], I. Nasteva[17], M. Needham[63], I. Neri[20], N. Neri[8,97], S. Neubert[103], N. Neufeld[11], R. Newcombe[30], T. D. Nguyen[27], C. Nguyen-Mau[27,104], E. M. Niel[18], S. Nieswand[33], N. Nikitin[36], N. S. Nolte[10], C. Nunez[7], A. Oblakowska-Mucha[70], V. Obraztsov[22], D. P. O'Hanlon[5], R. Oldeman[35,71], M. E. Olivares[23], C. J. G. Onderwater[68], A. Ossowska[41], J. M. Otalora Goicochea[17], T. Ovsiannikova[37], P. Owen[2], A. Oyanguren[89], B. Pagare[28], P. R. Pais[11], T. Pajero[45], A. Palano[65], M. Palutan[38], Y. Pan[14], G. Panshin[91], A. Papanestis[77], M. Pappagallo[65,66], L. L. Pappalardo[20,52], C. Pappenheimer[9], W. Parker[49], C. Parkes[14], C. J. Parkinson[4], B. Passalacqua[20], G. Passaleva[19], A. Pastore[65], M. Patel[30], C. Patrignani[57,58], C. J. Pawley[69], A. Pearce[11], A. Pellegrino[1], M. Pepe Altarelli[11], S. Perazzini[57], D. Pereima[37], P. Perret[6], M. Petric[11,12], K. Petridis[5], A. Petrolini[31,81], A. Petrov[96], S. Petrucci[63], M. Petruzzo[8], T. T. H. Pham[23], A. Philippov[24], L. Pica[34,105], M. Piccini[76], B. Pietrzyk[61], G. Pietrzyk[27], M. Pili[45], D. Pinci[100], F. Pisani[11], P. K. Resmi[25], V. Placinta[64], J. Plews[43], M. Plo Casasus[4], F. Polci[39], M. Poli Lener[38], M. Poliakova[23], A. Poluektov[25], N. Polukhina[32,106], I. Polyakov[23], E. Polycarpo[17], G. J. Pomery[5], S. Ponce[11], D. Popov[6,11], S. Popov[24], S. Poslavskii[22], K. Prasanth[41], L. Promberger[11], C. Prouve[4], V. Pugatch[73], H. Pullen[45], G. Punzi[29,105], W. Qian[56], J. Qin[56], R. Quagliani[39], B. Quintana[61], N. V. Raab[74], R. I. Rabadan Trejo[25], B. Rachwal[70], J. H. Rademacker[5], M. Rama[34], M. Ramos Pernas[28], M. S. Rangel[17], F. Ratnikov[24,47], G. Raven[90], M. Reboud[61], F. Redi[27], F. Reiss[14], C. Remon Alepuz[89], Z. Ren[62], V. Renaudin[45], R. Ribatti[34], S. Ricciardi[77], K. Rinnert[3], P. Robbe[18], G. Robertson[63], A. B. Rodrigues[27], E. Rodrigues[3], J. A. Rodriguez Lopez[102], A. Rollings[45], P. Roloff[11], V. Romanovskiy[22], M. Romero Lamas[4], A. Romero Vidal[4], J. D. Roth[7], M. Rotondo[38], M. S. Rudolph[23], T. Ruf[11], J. Ruiz Vidal[89], A. Ryzhikov[47], J. Ryzka[70], J. J. Saborido Silva[4], N. Sagidova[15], N. Sahoo[28], B. Saitta[35,71], M. Salomoni[11], D. Sanchez Gonzalo[13], C. Sanchez Gras[1], R. Santacesaria[100], C. Santamarina Rios[4], M. Santimaria[38], E. Santovetti[59,84], D. Saranin[32], G. Sarpis[12], M. Sarpis[103], A. Sarti[100], C. Satriano[100,107], A. Satta[59], M. Saur[10], D. Savrina[36,37], H. Sazak[6], L. G. Scantlebury Smead[45], S. Schael[33], M. Schellenberg[10], M. Schiller[12], H. Schindler[11], M. Schmelling[108], B. Schmidt[11], O. Schneider[27], A. Schopper[11], M. Schubiger[1], S. Schulte[27], M. H. Schune[18], R. Schwemmer[11], B. Sciascia[38], S. Sellam[4], A. Semennikov[37], M. Senghi Soares[90], A. Sergi[31], N. Serra[2], L. Sestini[40], A. Seuthe[10], P. Seyfert[11], Y. Shang[82], D. M. Shangase[7], M. Shapkin[22], I. Shchemerov[32], L. Shchutska[27], T. Shears[3], L. Shekhtman[48,79], Z. Shen[82], V. Shevchenko[96], E. B. Shields[53,54], E. Shmanin[32], J. D. Shupperd[23], B. G. Siddi[20], R. Silva Coutinho[2], G. Simi[40], S. Simone[65,66], N. Skidmore[14], T. Skwarnicki[23], M. W. Slater[43], I. Slazyk[20,52], J. C. Smallwood[45], J. G. Smeaton[16], A. Smetkina[37], E. Smith[33], M. Smith[30], A. Snoch[1], M. Soares[57], L. Soares Lavra[6], M. D. Sokoloff[9], F. J. P. Soler[12], A. Solovev[15], I. Solovyev[15], F. L. Souza De Almeida[17], B. Souza De Paula[17], B. Spaan[10], E. Spadaro Norella[8,97], P. Spradlin[12], F. Stagni[11], M. Stahl[9], S. Stahl[11], P. Stefko[27], O. Steinkamp[2,32], O. Stenyakin[22], H. Stevens[10], S. Stone[23], M. E. Stramaglia[27], M. Straticiuc[64], D. Strekalina[32], F. Suljik[45], J. Sun[35], L. Sun[42], Y. Sun[49], P. Svihra[14], P. N. Swallow[43], K. Swientek[70], A. Szabelski[83], T. Szumlak[70], M. Szymanski[11], S. Taneja[14], F. Teubert[11], E. Thomas[11], K. A. Thomson[3], V. Tisserand[6], S. T'Jampens[61], M. Tobin[60], L. Tomassetti[20,52], D. Torres Machado[29], D. Y. Tou[39], M. T. Tran[27], E. Trifonova[32], C. Trippl[27], G. Tuci[34,105], A. Tully[27], N. Tuning[1,11], A. Ukleja[83], D. J. Unverzagt[21], E. Ursov[32], A. Usachov[1], A. Ustyuzhanin[24,47], U. Uwer[21], A. Vagner[91], V. Vagnoni[57], A. Valassi[11], G. Valenti[57], N. Valls Canudas[55],

M. van Beuzekom[1], M. Van Dijk[27], E. van Herwijnen[32], C. B. Van Hulse[74], M. van Veghel[68], R. Vazquez Gomez[4], P. Vazquez Regueiro[4], C. Vázquez Sierra[11], S. Vecchi[20], J. J. Velthuis[5], M. Veltri[19,109], A. Venkateswaran[23], M. Veronesi[1], M. Vesterinen[28], D. Vieira[9], M. Vieites Diaz[27], H. Viemann[101], X. Vilasis-Cardona[55], E. Vilella Figueras[3], P. Vincent[39], D. Vom Bruch[25], A. Vorobyev[15], V. Vorobyev[48,79], N. Voropaev[15], R. Waldi[101], J. Walsh[34], C. Wang[21], J. Wang[82], J. Wang[60], J. Wang[62], J. Wang[42], M. Wang[62], R. Wang[5], Y. Wang[87], Z. Wang[2], Z. Wang[62], H. M. Wark[3], N. K. Watson[43], S. G. Weber[39], D. Websdale[30], C. Weisser[46], B. D. C. Westhenry[5], D. J. White[14], M. Whitehead[5], D. Wiedner[10], G. Wilkinson[45], M. Wilkinson[23], I. Williams[16], M. Williams[46], M. R. J. Williams[63], F. F. Wilson[77], W. Wislicki[83], M. Witek[41], L. Witola[21], G. Wormser[18], S. A. Wotton[16], H. Wu[23], K. Wyllie[11], Z. Xiang[56], D. Xiao[87], Y. Xie[87], A. Xu[82], J. Xu[56], L. Xu[62], M. Xu[87], Q. Xu[56], Z. Xu[82], Z. Xu[56], D. Yang[62], S. Yang[56], Y. Yang[56], Z. Yang[62], Z. Yang[49], Y. Yao[23], L. E. Yeomans[3], H. Yin[87], J. Yu[110], X. Yuan[23], O. Yushchenko[22], E. Zaffaroni[27], M. Zavertyaev[106,108], M. Zdybal[41], O. Zenaiev[11], M. Zeng[62], D. Zhang[87], L. Zhang[62], S. Zhang[82], Y. Zhang[82], Y. Zhang[45], A. Zhelezov[21], Y. Zheng[56], X. Zhou[56], Y. Zhou[56], X. Zhu[62], Z. Zhu[56], V. Zhukov[33,36], J. B. Zonneveld[63], Q. Zou[60], S. Zucchelli[57,58], D. Zuliani[40] and G. Zunica[14]

[1]Nikhef National Institute for Subatomic Physics, Amsterdam, Netherlands. [2]Physik-Institut, Universität Zürich, Zürich, Switzerland. [3]Oliver Lodge Laboratory, University of Liverpool, Liverpool, UK. [4]Instituto Galego de Física de Altas Enerxías (IGFAE), Universidade de Santiago de Compostela, Santiago de Compostela, Spain. [5]H.H. Wills Physics Laboratory, University of Bristol, Bristol, UK. [6]Université Clermont Auvergne, CNRS/IN2P3, LPC, Clermont-Ferrand, MI, France. [7]University of Michigan, Ann Arbor, USA. [8]INFN Sezione di Milano, Milano, Italy. [9]University of Cincinnati, Cincinnati, OH, USA. [10]Fakultät Physik, Technische Universität Dortmund, Dortmund, Germany. [11]European Organization for Nuclear Research (CERN), Geneva, Switzerland. [12]School of Physics and Astronomy, University of Glasgow, Glasgow, UK. [13]ICCUB, Universitat de Barcelona, Barcelona, Spain. [14]Department of Physics and Astronomy, University of Manchester, Manchester, UK. [15]Petersburg Nuclear Physics Institute NRC Kurchatov Institute (PNPI NRC KI), Gatchina, Russia. [16]Cavendish Laboratory, University of Cambridge, Cambridge, UK. [17]Universidade Federal do Rio de Janeiro (UFRJ), Rio de Janeiro, Brazil. [18]Université Paris-Saclay, CNRS/IN2P3, IJCLab, Orsay, France. [19]INFN Sezione di Firenze, Firenze, Italy. [20]INFN Sezione di Ferrara, Ferrara, Italy. [21]Physikalisches Institut, Ruprecht-Karls-Universität Heidelberg, Heidelberg, Germany. [22]Institute for High Energy Physics NRC Kurchatov Institute (IHEP NRC KI), Protvino, Russia. [23]Syracuse University, Syracuse, NY, USA. [24]Yandex School of Data Analysis, Moscow, Russia. [25]Aix Marseille Univ, CNRS/IN2P3, CPPM, Marseille, France. [26]Laboratoire Leprince-Ringuet, CNRS/IN2P3, Ecole Polytechnique, Institut Polytechnique de Paris, Palaiseau, France. [27]Institute of Physics, Ecole Polytechnique Fédérale de Lausanne (EPFL), Lausanne, Switzerland. [28]Department of Physics, University of Warwick, Coventry, UK. [29]Centro Brasileiro de Pesquisas Físicas (CBPF), Rio de Janeiro, Brazil. [30]Imperial College London, London, UK. [31]INFN Sezione di Genova, Genova, Italy. [32]National University of Science and Technology 'MISIS', Moscow, Russia. [33]I. Physikalisches Institut, RWTH Aachen University, Aachen, Germany. [34]INFN Sezione di Pisa, Pisa, Italy. [35]INFN Sezione di Cagliari, Monserrato, Italy. [36]Institute of Nuclear Physics, Moscow State University (SINP MSU), Moscow, Russia. [37]Institute of Theoretical and Experimental Physics NRC Kurchatov Institute (ITEP NRC KI), Moscow, Russia. [38]INFN Laboratori Nazionali di Frascati, Frascati, Italy. [39]LPNHE, Sorbonne Université, Paris Diderot Sorbonne Paris Cité, CNRS/IN2P3, Paris, France. [40]Universita degli Studi di Padova, Universita e INFN, Padova, Padova, Italy. [41]Henryk Niewodniczanski Institute of Nuclear Physics Polish Academy of Sciences, Kraków, Poland. [42]School of Physics and Technology, Wuhan University, Wuhan, China. [43]University of Birmingham, Birmingham, UK. [44]Università di Modena e Reggio Emilia, Modena, Italy. [45]Department of Physics, University of Oxford, Oxford, UK. [46]Massachusetts Institute of Technology, Cambridge, MA, USA. [47]National Research University Higher School of Economics, Moscow, Russia. [48]Budker Institute of Nuclear Physics (SB RAS), Novosibirsk, Russia. [49]University of Maryland, College Park, MD, USA. [50]Guangdong Provencial Key Laboratory of Nuclear Science, Institute of Quantum Matter, South China Normal University, Guangzhou, China. [51]Institute for Nuclear Research of the Russian Academy of Sciences (INR RAS), Moscow, Russia. [52]Università di Ferrara, Ferrara, Italy. [53]INFN Sezione di Milano-Bicocca, Milano, Italy. [54]Università di Milano Bicocca, Milano, Italy. [55]DS4DS, La Salle, Universitat Ramon Llull, Barcelona, Spain. [56]University of Chinese Academy of Sciences, Beijing, China. [57]INFN Sezione di Bologna, Bologna, Italy. [58]Università di Bologna, Bologna, Italy. [59]INFN Sezione di Roma Tor Vergata, Roma, Italy. [60]Institute Of High Energy Physics (IHEP), Beijing, China. [61]Univ. Savoie Mont Blanc, CNRS, IN2P3-LAPP, Annecy, France. [62]Center for High Energy Physics, Tsinghua University, Beijing, China. [63]School of Physics and Astronomy, University of Edinburgh, Edinburgh, UK. [64]Horia Hulubei National Institute of Physics and Nuclear Engineering, Bucharest-Magurele, Romania. [65]INFN Sezione di Bari, Bari, Italy. [66]Università di Bari, Bari, Italy. [67]Los Alamos National Laboratory (LANL), Los Alamos, NM, USA. [68]Van Swinderen Institute, University of Groningen, Groningen, Netherlands. [69]Universiteit Maastricht, Maastricht, Netherlands. [70]Faculty of Physics and Applied Computer Science, AGH University of Science and Technology, Kraków, Poland. [71]Università di Cagliari, Cagliari, Italy. [72]Eotvos Lorand University, Budapest, Hungary. [73]Institute for Nuclear Research of the National Academy of Sciences (KINR), Kyiv, Ukraine. [74]School of Physics, University College Dublin, Dublin, Ireland. [75]NSC Kharkiv Institute of Physics and Technology (NSC KIPT), Kharkiv, Ukraine. [76]INFN Sezione di Perugia, Perugia, Italy. [77]STFC Rutherford Appleton Laboratory, Didcot, UK. [78]School of Physics and Astronomy, Monash University, Melbourne, Victoria, Australia. [79]Novosibirsk State University, Novosibirsk, Russia. [80]Department of Physics and Astronomy, Uppsala University, Uppsala, Sweden. [81]Università di Genova, Genova, Italy. [82]School of Physics State Key Laboratory of Nuclear Physics and Technology, Peking University, Beijing, China. [83]National Center for Nuclear Research (NCBJ), Warsaw, Poland. [84]Università di Roma Tor Vergata, Roma, Italy. [85]Pontifícia Universidade Católica do Rio de Janeiro (PUC-Rio), Rio de Janeiro, Brazil. [86]Universidade Federal do Triângulo Mineiro (UFTM), Uberaba-MG, Brazil. [87]Institute of Particle Physics, Central China Normal University, Wuhan, China. [88]Hangzhou Institute for Advanced Study, UCAS, Hangzhou, China. [89]Instituto de Fisica Corpuscular, Centro Mixto Universidad de Valencia - CSIC, Valencia, Spain. [90]Nikhef National Institute for Subatomic Physics and VU University Amsterdam, Amsterdam, Netherlands. [91]National Research Tomsk Polytechnic University, Tomsk, Russia. [92]Faculty of Computer Science, Electronics and Telecommunications, AGH University of Science and Technology, Kraków, Poland. [93]Università di Siena, Siena, Italy. [94]Università di Padova, Padova, Italy. [95]Scuola Normale Superiore, Pisa, Italy. [96]National Research Centre Kurchatov Institute, Moscow, Russia. [97]Università degli Studi di Milano, Milano, Italy. [98]MSU–Iligan Institute of Technology (MSU-IIT), Iligan, Philippines. [99]Università di Firenze, Firenze, Italy. [100]INFN Sezione di Roma La Sapienza, Roma, Italy. [101]Institut für Physik, Universität Rostock, Rostock, Germany. [102]Departamento de Fisica, Universidad Nacional de Colombia, Bogota,

Colombia. [103]Universität Bonn Helmholtz-Institut für Strahlen und Kernphysik, Bonn, Germany. [104]Hanoi University of Science, Hanoi, Vietnam. [105]Università di Pisa, Pisa, Italy. [106]P.N. Lebedev Physical Institute, Russian Academy of Sciences (LPI RAS), Moscow, Russia. [107]Università della Basilicata, Potenza, Italy. [108]Max-Planck-Institut für Kernphysik (MPIK), Heidelberg, Germany. [109]Università di Urbino, Urbino, Italy. [110]Physics and Micro Electronic College, Hunan University, Changsha City, China. ✉e-mail: alessandro.bertolin@pd.infn.it